Performance Analysis of Cervical Cancer Detection System Using Fusion Based CFICNN Classifier

I. Dhurga bai[1]*, and A. Selvapandian[2]
[1] Assistant Professor, Department of Electronics and Communication Engineering,
Theni Kammavar Sangam College of Technology, India
[e-mail: idhurgabaiphd@gmail.com]
[2] Associate Professor, Department of Electronics and Communication Engineering,
Gnanamani College of Technology, India.
[e-mail: selvapandian@gct.org.in]
*Corresponding author: I. Dhurga bai

Received March 18, 2024; revised September 10, 2024; accepted October 7, 2024; published October 31, 2024

Abstract

This paper proposes a fully computer assisted automated cervical cancer detection method using cervical images. This proposed system consist of six modules as Edge detector, image fusion, Gabor transform, feature computation, classification algorithm and segmentation method. The edge pixels show the contrast edge variations of each pixel in cervical image with respect to its corresponding nearby pixels. Hence, these edge pixels are detected using fuzzy logic and then the edge detected cervical images are fused using arithmetic pixel fusion algorithm. This fused cervical image having the pixels in the form of spatial resolution and hence it is need to be converted into multi-format resolution for computing the features from it. The spatial pixels in fused image are converted into multi orientation pixels using Gabor transform and then features are computed from this Gabor image. In this work, Local Binary Pattern (LBP), Grey Level Co-occurrence Matrix (GLCM) and Pixel Intensity Features (PIF) are computed from the Gabor cervical image. These features have been classified by the Cervical Features Incorporated Convolutional Neural Networks (CFICNN) classification algorithm. The modified version of the Visual Geometry Group- Convolutional Neural Networks (VGG-CNN) architecture is called as Cervical Features Incorporated CNN (CFICNN) and it is proposed in this paper for both training and classification process. Finally, the cancer pixels are segmented using morphological operations based segmentation algorithm. The Guanacaste Dataset (GD) and Kaggle Dataset (KD) are used for estimating performance efficiency.

Keywords: Cancer, Cervical, Classifications, Dataset, Features.

http://doi.org/10.3837/tiis.2024.10.007 **ISSN : 1976-7277**

1. Introduction

The cancer cells are developed in anywhere of the human body to various reasons such as genetic disorder, food habits, and life style changes. These cancer cells in the human body gradually increases and affects the performance and functions of the surrounding cells. The cancer disease is affected both male and female irrespective of their sex. Apart from men cancer, the women are severely affected by various cancer diseases. Among these cancer types, cervical cancer and breast cancer are identified as most important cancer and leads to death in women patients [1-3]. Hence, there detection is important to prevent death in women patients. Among these two cancer types, breast cancers are known as externally affected disease category and the death ratio is very less when compared with the other cervical cancer type. The cervical cancer is known as internally affected disease category and the death ratio of the affected patient is high when compared with breast cancer. Moreover, its prediction level is significantly low when compared with the prediction level of the breast cancer. Hence, it is important to identify the cervical cancer at an earlier stage [4-5]. In this paper, the cervical cancer can be screened using cervical images using deep learning methods. **Fig. 1(a)** shows the Cervigram belonging to healthy and **Fig. 1(b)** shows the Cervigram belonging to cancer.

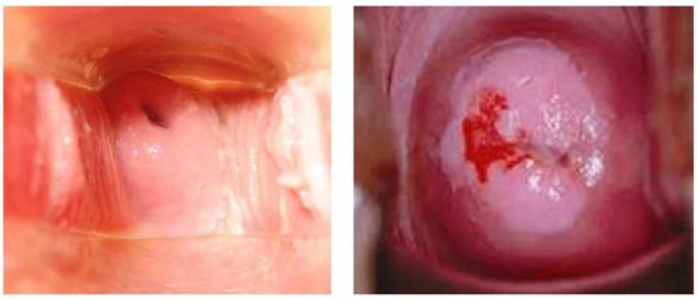

Fig. 1. (a) Cervigram belonging to healthy (b) Cervigram belonging to cancer

Mathivanan et al. (2024) proposed fusion logic in deep learning classification method to identify the abnormal pixel locations in the cervical image. Inception v3 and Resnet, two different deep learning models, were combined to increase the diagnosis rate of cervical cancer. The suggested methodology was examined and verified by the authors using cervical images from the SIPaKMeD dataset in order to confirm its robustness with regard to different indexing values. The mean classification accuracy about 98% was obtained by this method. Nitin Kumar Chauhan et al. [7] detected the abnormalities through the cancer segmentation method using image diagnosis process in this work. They attained an novel hybrid deep network model for the classification process and developed segmentation algorithm for identification any abnormalities in the cervical regions of the women patients. In this work, the authors applied various deep learning algorithms such as Visual Geometry Group (VGG), ResNET and DenseNet individually on the cervical images to obtain the experimental results. They attained 95.3% Detection Rate (DI) of the cancer region detection process using VGG classifier and the authors obtained 92.38% DI of the cancer region detection process using ResNET classifier. They attained 96.1% DI of the cancer region detection process using DenseNet classifier. Glučina et al. [15] developed an cervical cancer screening method using the machine learning algorithms such as Multilayer Perception (MP), SVM and K-Nearest Neighbor (KNN)

approaches in this paper. The individual performance of the each machine learning algorithm was analyzed in this work with respect to its classification index parameter. They attained 95.2% DI of the cancer region detection process using MP classifier and they attained 96.1% of classification accuracy of the cancer region detection process using SVM classifier. The authors obtained 97.3% DI of the cancer region detection process using KNN classifier. Umesh Kumar Lilhore et al. [8] implemented numerous logical modeling methods and classifying the images. The boruta analysis techniques were used in this work to select the region of investigated pixels and the comprehensive feature lists were derived from this region of investigated pixels. Then, the authors used Support Vector Machine (SVM) method to optimize the selected investigated group and Pap smear images to classify the region of interest into either normal or abnormal. The experimental results were validated by standard testing approaches in this work with other existing methods.

Park et al. [11] analyzed the implementation results for the cervical cancer using various machine and deep learning modeling approaches. Using cervicography imaging methods, the authors compared the experimental results of both machine and deep learning modeling approach for both classifying process and the abnormal region segmentation process on the large set of cervical images in this work. Finally, the k-fold validation models were applied on the experimental results of machine and deep learning modeling individually to identify the suitable methods. To locate the area of cancer pixels in the cervical pictures, Charoenkwan et al. [13] built and developed an automated Parametrial Cancer Invasion (PCI) model. The authors used clinicopathological data for the effective testing of the developed PCI model in this paper. The Random Forest (RF) computational and classification algorithm was used in this work for computing feature regions from the cervical image. They had used 10-fold cross validation algorithm on the experimental results of the developed PCI model to validate the test experimental results in this paper. Patil et al. [14] predicted the various risk factors and constrained modeling based machine learning algorithms for the prediction process in this work. Finally, the experimental results of the risk factor prediction models were analyzed and tested through the various folding algorithms in this work. The comparative analysis was done on the various machine learning modeling algorithms on various cervical image dataset in this paper to validate the experimental results. Dong et al. (2020) classified the cervical Pap smear cell images using Inception v3 model through the combination of external and internal metric and statistic features. Hua et al. (2020) predicted the level of cervical cancer in both histopathological cell images and cervigram images using multi featuring deep learning algorithm. This computation of multi level features in deep learning models improved the cervical cancer detection rate. The mean classification accuracy about 97.9% was obtained by this method.

Aina et al. [16] presented and reviewed a number of deep learning models-based techniques for cervical cancer diagnosis. In order to validate the suggested algorithms based on the experimental outcomes of the traditional deep learning models in this study, the authors compared the importance of each deep learning model. The experimental results with respect to classification rate which have been utilized by the authors to compare the individual performance of each deep learning models in this work. Wu et al. [17] used cytological images to identify the region of pixels belonging to the cancer using deep learning algorithms. The results of each method were significantly compared with other similar deep learning models in this work. Wu et al. (2018) used cytological images to identify the region of pixels belonging to the cancer using deep learning algorithms. The results of each method were significantly compared with other similar deep learning models in this work.

From the extensive study of the conventional approaches, the following novelties have been proposed.

- A novel pixel based image fusion method is proposed to detect the edge pixels in cervical images using the constructed Fuzzy Logic Approach (FLA).
- Cervical Features Incorporated CNN (CFICNN) classification algorithm has been proposed for the classification process.

2. Proposed Methodology

In this study, an automated technique for entirely computer assisted detection of cervical cancer utilizing pictures of the cervical region has been proposed. **Fig. 2(a)** shows the Proposed CFICNN system (training) and **Fig. 2(b)** shows the proposed CFICNN system (testing).

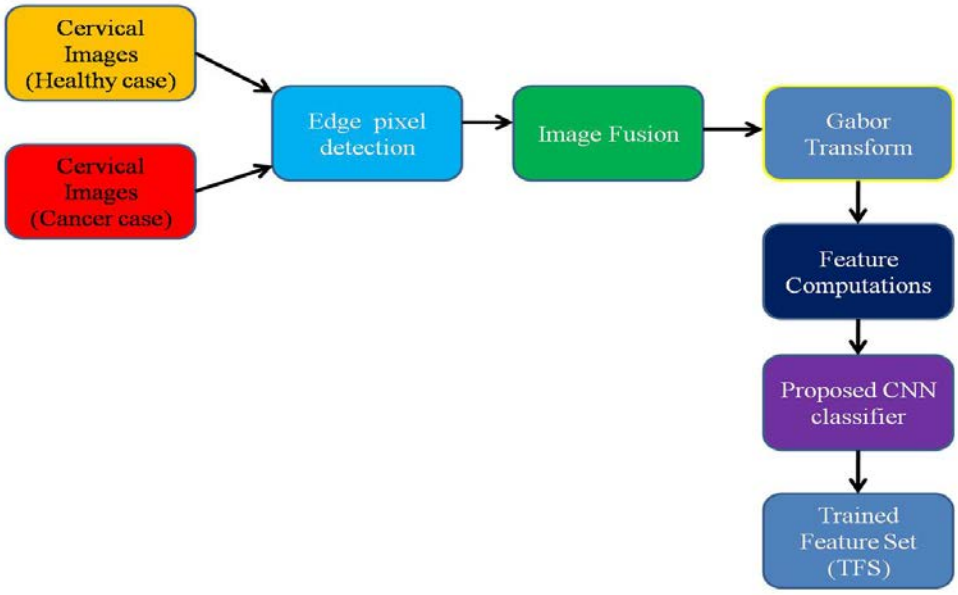

(a)

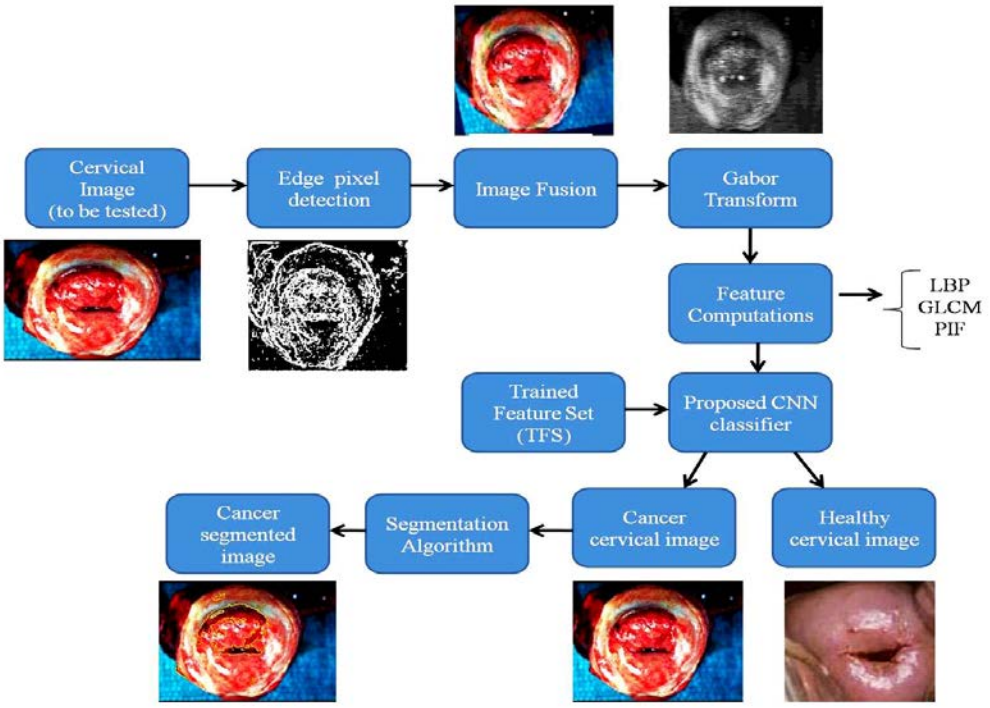

(b)

Fig. 2. (a) Proposed CFICNN based cervical cancer detection system (training)
(b) Proposed CFICNN based cervical cancer detection system (testing)

2.1 Datasets

In this paper, Guanacaste Dataset (GD) and Kaggle Dataset (KD) are used for functional estimation of the proposed system. Both the dataset images are publicly available with license free agreement and hence the researchers in this field can use the cervical images from these two datasets for their research works. The National Cancer Institute (NCI) created and organized the cervical images in this GD and it was constructed in the year of 1997. The organizer of this dataset updates the cervical images in this open access dataset every year by including recent cervical images which are obtained through various medical screening programmes around the number of health centers in world. This GD contains two types of cervical images under the category of healthy and cancer. From this GD, 1500 cervical images are obtained and they are classified into 750 healthy case and 750 cancer case cervical images respectively. In this paper, training and testing ratio is set to 20:80 and hence 150 healthy images have been trained and the remaining 600 healthy images have been tested.

In addition to this work, the cervical images in KD was constructed and collected through Mobile ODT application in Visual Assessment mode. The KD contains 1960 cervical images and these cervical images are categorized into 1448 training case images and 512 testing case images. The training cervical images are further sub categorized as 1158 healthy case images and 290 cancer case images. The testing cervical images are further sub categorized as 410 healthy case images and 102 cancer case images. The image size in GD is about 512 ×512 as

image width and height pixel resolution and the image size in KD is about 256×256 as image width and height respectively. These two dataset also have Gold Standard (GS) cervical images which are obtained through the two independent radiologists in this field. These GS images have been used for computing the efficiency of the proposed system.

2.2 Edge detection and fusion

The image fusion algorithm enhances the intensity of each pixel in cervical image to improve the cancer pixel detection rate. The edges show the pixel differentiation between the healthy and cancer pixels in cervical image. In traditional enhancement methods such as Histogram Equalization and Local Adaptive Histogram Equalization, used non-overlapping region window to enhance the pixels within this window. These methods enhanced all the pixels lies within this selected window. This means that all the pixels belonging to both cancer and non-cancer pixels which are in the region of the window have been enhanced. Hence, the difference between the enhanced cancer pixels and enhanced non-cancer pixels have not been identified which creates a complexity in the cervical image classification process. Moreover, the time complexity of these traditional enhancement algorithms is high due to the enhancement of all pixel values. These limitations of these traditional enhancement processes are overcome by using edge based fusion algorithm.

The edges show the pixel differentiation between the healthy and cancer pixels in cervical image. The conventional image fusion method fuses all the pixels in two cervical images with respect to corresponding coordinates to produce the fused cervical image. This approach enhances all the pixels in the source cervical image which were not be useful for differentiating the cancer pixels and the healthy pixels in cervical image. Hence, this paper proposes edge detection based fusion approach which initially detects the edge pixels in cervical images and then applies the fusion algorithm on the detected edge pixels only to differentiate the cancer and healthy pixels for further processing, as proposed as a novel technique. In this paper, FLA is used to detect the edge pixels in source cervical image. This proposed FLA uses set of fuzzy rules to identify the edge pixels. This FLA method uses 2×2 mask where all the elements in this mask are loaded with the pixels from the source cervical image. This 2×2 mask region is depicted in the following **Fig. 3**.

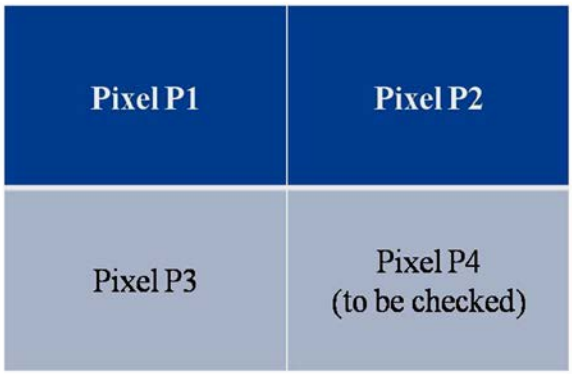

Fig. 3. Mask in proposed FLA

In **Fig. 3**, four pixels P1, P2, P3 and P4 are considered and the fourth pixel P4 is to be checked for edge pixel. This fourth pixel P4 is linearly correlated with the other pixels P1, P2 and P3. Hence, the variations between the pixel P4 and the other pixels P1, P2 and P3 are used to detect whether pixel P4 is belonging to edge pixel or not. In the proposed FLA, 2^n rules are

constructed, where ‘n’ is the number of pixels in 2×2 mask region. In this work, four pixels (n=4) are considered for identifying the fourth pixel to be edge pixel. Therefore, 16 fuzzy rules are employed in this work for this 2×2 mask region to identify the fourth pixel P4 to be edge or not.

The histogram value of the source cervical image is computed and its average value is considered as threshold value. Each pixel in the source cervical image is compared with the value of this computed threshold. A pixel in the source cervical picture is regarded as "0" throughout the fuzzy rule creation procedure if its value is greater than or equal to the threshold. If the pixel value is lesser than the value of the threshold, then that pixel is considered as ‘1’ for fuzzy rules construction process. By applying this procedure to all the pixels, the source cervical RGB image is converted into binary image, which consists of ‘0’s and ‘1’s. **Table 1** shows the Construction of fuzzy rules in the proposed FLA. In this table, the value of each pixel is considered as either ‘0’ or ‘1’. The variation of pixel value in P4 with respect to other surrounding correlation pixels are used in the construction of fuzzy rules in the proposed FLA. The fourth pixel P4 is identified as ‘edge pixel’ if there is a variation of the pixel value between the pixel P4 and with respect to any of its surrounding pixel values. The fourth pixel P4 is identified as ‘No edge pixel’ if there is no variation of the pixel value between the pixel P4 and with respect to any of its surrounding pixel values.

Table 1. Construction of fuzzy rules in the proposed FLA

Pixel P1	Pixel P2	Pixel P3	Pixel P4	Status of Pixel P4
0	0	0	0	No edge
0	0	0	1	Edge
0	0	1	0	Edge
0	0	1	1	Edge
0	1	0	0	Edge
0	1	0	1	Edge
0	1	1	0	Edge
0	1	1	1	Edge
1	0	0	0	Edge
1	0	0	1	Edge
1	0	1	0	Edge
1	0	1	1	Edge
1	1	0	0	Edge
1	1	0	1	Edge
1	1	1	0	Edge
1	1	1	1	No edge

In this paper, the properties of each rule have to be set with respect to fuzzy logic method. In FLA, two different ruling approaches are followed as ‘Mamdani’ and ‘Sugeno’. The mamdani FLA is mostly used to imaging applications where the sugeno FLA is mostly used to signal processing applications. Hence, this paper uses mamdani FLA method to detect the edge pixels. In this mamdani FLA method, the membership function with the triangular property is set for all the pixels and the 2×2 mask region are having two membership functions (mf1 and mf2) with triangular property. The final status of the pixel P4 have three membership functions as mf1 for pixel ‘0’, mf2 for pixel ‘edge’ and mf3 for pixel ‘1’.

In this paper, the proposed FLA method applies two consecutive times on the source cervical image. The thick edge pixels have been identified during the first iteration of the FLA method and the thin edge have been identified during the second iteration of the FLA method.

Fig. 4(a) shows the cervical image, **Fig. 4(b)** shows the thick edge pixels identified cervical image and **Fig. 4(c)** shows the thin edge pixels identified cervical image.

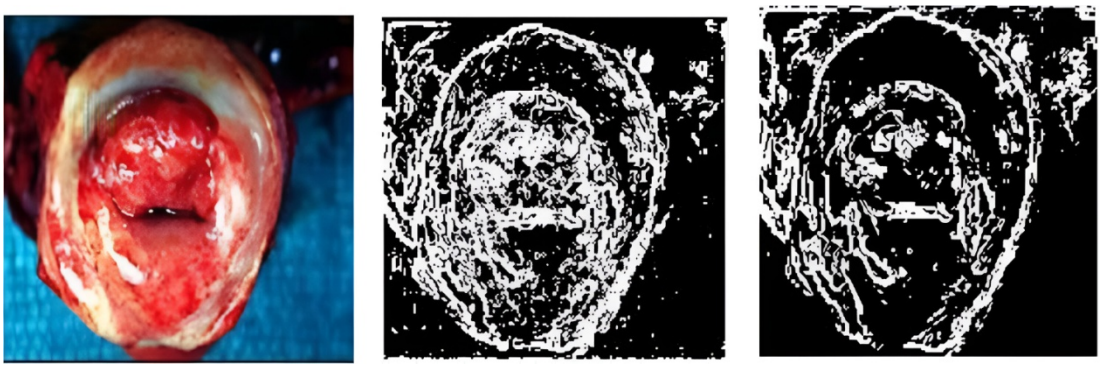

(a) **(b)** **(c)**

Fig. 4. Edge detected cervical image (a) Thick edge pixels (b) Thin edge pixels

Further, image fusion method is applied between the thick edge detected image and thin edge detected cervical images. In this paper, Arithmetic Addition (AA) method is used as pixel level image fusion approach, where the corresponding pixels in both thick and thin edge detected images are fused (arithmetic added) to produce the enhanced cervical image, as illustrated in **Fig. 5**.

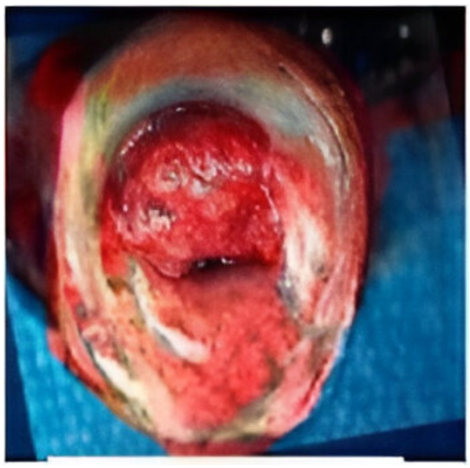

Fig. 5. Enhanced cervical image

2.3 Gabor Transformation

In this paper, linear filter has been used on the pre-processed output which is used for transforming the pixels (which are belonging to time series) to the frequency centered pixels. For this purpose, Gabor filter is used in this work which is one type of linear filter with various kernel size. The kernel of the Gabor filter is functioned based on the central frequency and orientation. This kernel of Gabor filter is convolved with the preprocessed cervical image for the process of transformation of pixels with respect to frequency pattern. The kernel in the form of one dimensional is the main reason for performing the linear convolution during the pixel transformations, as depicted in Equation (1).

$$G(f_{0,}\theta) = \frac{{f_0}^2}{\pi\gamma} \times e^{-\left(\frac{{f_0}^2 * x1^2}{\gamma} + \frac{{f_0}^2 * y1^2}{\gamma}\right)} \times Cos\,(2\pi f_0 x1\,\theta) + Sin\,(2\pi f_0 y1\,\theta) \quad (1)$$

Whereas, f_0 is depicted as central frequency, (x1, y1) are the geometric coordination of Gabor kernel, $\theta\ is$ the orientation of Gaussian operator, γ is represented as aspect ratio which denotes the elasticity of the Gaussian operator.

The spatial geometric coordinates of the Gabor kernel is given in the following equations.

$$x1 = x\cos\theta + y\ sin\theta \quad (2)$$

$$y1 = y\cos\theta - x\ sin\theta \quad (3)$$

The Gabor response is entirely based on the Gabor filter central frequency and orientation. These two parameters plays the major role for transforming the pixels in the preprocessed cervical image. The size of the Gabor kernel in Gabor filter determines the non-linearity in the output transformed image. In order to significantly reduce the non-linearity in the output of the Gabor filter, its kernel is set to be small. In this paper, the Gabor filter with 3*3 sized Gabor kernel is used and it is multiplied by the preprocessed cervical image using the following equation.

$$Cervical_{transformed} = I\,(x, y) \times \{G(f_{0,}\theta), 3 \times 3\} \quad (4)$$

Fig. 6 shows the cervical picture modified using Gabor.

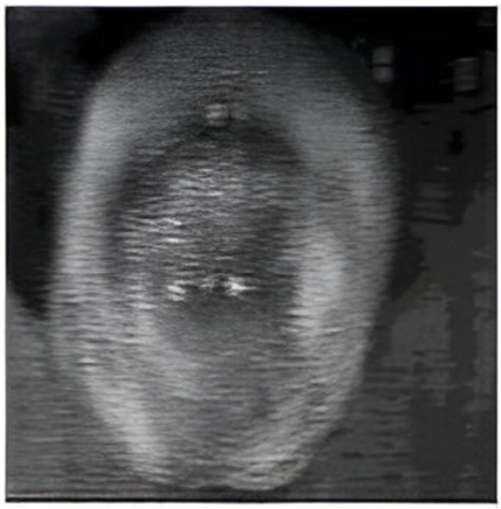

Fig. 6. Gabor transformed cervical image

2.4 Feature Extractions

In order to distinguish each pixel in the Gabor transformed cervical picture from the surrounding pixel intensity values, the feature values reflect the correlation of each pixel value. Consequently, the attributes have been deployed for differentiating between the abnormal and healthy cervical images. This paper computes statistical and pixel variance features using LBP, GLCM, and PIF feature parameters. The computations of these feature values are entirely dependent on the surrounding pixel intensity values. These feature computation process is illustrated in the following sections.

2.4.1 Computations of Local Binary Pattern (LBP) features

These two pixel intensity features are computed for each pixel (feature to be computed) and the LBP produces single feature value for a single pixel intensity of the Gabor transformed cervical image. Therefore these two feature computations are called as binary index features. The computation of LBP for each pixel intensity value as illustrated in the steps.

Step 1:

Construct Index Window Mask (IWM) with three rows and columns with empty value.

Step 2:

Place this constructed IWM on the first pixel intensity of the Gabor transformed cervical image, where the first pixel intensity is centric in the IWM.

Step 3:

The value of the centric pixel intensity in IWM is compared with all of its surrounding pixel intensity values based on the decimal intensity comparison method.

Step 4:

The value of each surrounding intensity pixel value is changed to the high binary value (1) or low binary value (0) based on the following constraints.

$$IWM(Sp) = \begin{cases} 1; if\ sp \geq Cp \\ 0; else \end{cases} \quad (5)$$

Whereas, sp and Cp are the surrounding pixel value and centric pixel value in IWM.

Step 5:

The newly constructed IWM without center value is multiplied with the following Decimal Window Mask (DWM).

$$DWM = \begin{bmatrix} 8 & 4 & 2 \\ 16 & 0 & 1 \\ 32 & 64 & 128 \end{bmatrix}$$

The LBP value of the IWM is computed by multiplying the IWM values and the above DWM values as illustrated in the following equation.

$$LBP\ (Cp\ in\ IWM) = IWM \times DWM \quad (6)$$

Step 6:

Move the empty IWM to the next centric pixel value and repeat the steps from 1 to 5 till the end of the pixel in the Gabor transformed cervical image and the computed LBP image is shown in **Fig. 7**.

Fig. 7. Computed LBP image

2.4.2 Computations of Grey Level Co-occurrence Matrix (GLCM) features

The Gabor picture is used to compute the GLCM features at a 45-degree phase orientation of the pixels. The properties of energy, contrast, correlation, and homogeneity are computed from the GLCM matrix. When the suggested classifier is being trained, these features are separately computed from the normal and abnormal cervical images to create training sequences in addition to the other features. As shown in **Table 2**, these GLCM features are employed to distinguish between the aberrant and normal cervical images.

Table 2. Computation values of GLCM

Features	Computed values	
	Normal cervical image	**Abnormal cervical image**
Energy	1.23×10^{2}	3.9×10^{2}
Contrast	5.6×10^{3}	1.3×10^{3}
Correlation	1.89×10^{-2}	8.3×10^{-3}
Homogeneity	5.9×10^{4}	-1.2×10^{3}

2.4.3 Pixel Intensity Feature

The pixels in Gabor cervical image are stored in a vector matrix whose rows and columns are equals to the size of the Gabor cervical image. From this vector matrix V(x,y) , the following pixel intensity features are computed.

$$Pixel\ Energy\ Feature\ (PEF) = \frac{\sum_{x=1}^{M}\sum_{y=1}^{N}V(x,y)^2}{M\times N} \quad (7)$$

Where, M and N are the size of the vector matrix $V(x,y)$. i.e., rows and column representation.

$$Pixel\ Row\ Index\ Rate\ (PRIR) = \frac{\sum_{x=1}^{M}\sum_{y=1}^{N}V(x,y)^2}{M} \quad (8)$$

$$Pixel\ Column\ Index\ Rate\ (PCIR) = \frac{\sum_{x=1}^{M}\sum_{y=1}^{N}V(x,y)^2}{N} \quad (9)$$

$$Pixel\ Mean\ Feature\ (PMF) = \sum_{x=1}^{M}\sum_{y=1}^{N}V(x,y) \quad (10)$$

The above derived PEF, PRIR, PCIR and PMF features have been used to differentiate the healthy and non-healthy case during training of the proposed classification algorithm and the similar set of PIF are computed from the source test cervical image during its test mode classification process in this paper.

2.5 CNN classifications

The computed features are integrated into single matrix whose rows and columns are set to M and N and this two dimensional matrix is derived from both normal and abnormal cervical images during the training process of classification algorithm. The proposed structure is structured which is the modification of the conventional VGG-CNN architecture, for training and classification of the computed features. The modified version of the VGG-CNN architecture is called as Cervical Features Incorporated CNN (CFICNN) and it is proposed in this paper for both training and classification process. During training stage of this proposed CFICNN algorithm, the two dimensional matrix is computed from both normal and abnormal cervical images and these matrix are fed into the proposed CFICNN architecture to produce the Training Sequences (TS). This TS is used in testing process of the proposed CFICNN

architecture along with the two dimensional features from the test cervical image in this paper. In existing VGG-16 deep learning algorithm, 13 numbers of Convolutional layers(Conv), five numbers of Pooling layers (pooling) and three numbers of dense layers (neural network) are used. This entire architecture receives the TS from both normal and abnormal (cancer) cervical images which is available in training dataset. All the internal layers in this existing deep learning algorithm are connected in the form of sequential and hence each layer input is entirely based on the previous layer output. Hence, this existing CNN architecture consumes more classification and computational time period for the large number of cervical images in training dataset with respect to both normal and abnormal category of cervical images. This is the main drawback of this existing VGG-16 deep learning algorithm for the detection of cervical cancer images from the normal cervical images. Hence, this structure requires modification of the internal layers which are to be connected in the form of the parallel and hence the proposed CFICNN deep learning algorithm is developed in this paper to overcome the drawbacks of the existing VGG-16 deep learning model.

The Convolutional layer in VGG-16 deep learning algorithm is used to produce the internal features from the external features through the two dimensional Convolution process. In this existing design of the CNN, all the Convolutional layers are configured in sequential and hence less number of these layers are used in this design. This leads to the development of the proposed design for feature classifications for cervical image classifications in this paper. The proposed CFICNN deep learning model is operated in two parallel configurations of phases for the classifications of the cervical images into either normal or abnormal. The proposed CFICNN architecture is designed with 15 numbers of Convolutional layers(Conv), six numbers of Pooling layers (pooling) and three numbers of dense layers (neural network). In phase 1 of the proposed CFICNN design, six numbers of Convolutional layers are incorporated and nine numbers of Convolutional layers are incorporated in phase-2 of the proposed CFICNN design. More number of internal features increases the classification rate of the cervical images. Therefore, this proposed design uses more numbers of Convolutional layers than the existing design for cervical image classification process. The Convolutional layer in this proposed CFICNN design is represented by the notation C and the pooling layer is represented by the notation P and the dense layer is represented by the notation DE.

Figs 8(a) and **8(b)** depict the current VGG-16 deep learning model and the suggested CFICNN deep learning model, respectively, for the feature classification process in the detection of cervical cancer images. **Table 3** shows the number of convolutional, pooling, and dense layers as well as the number of internal filters utilized in each convolutional layer.

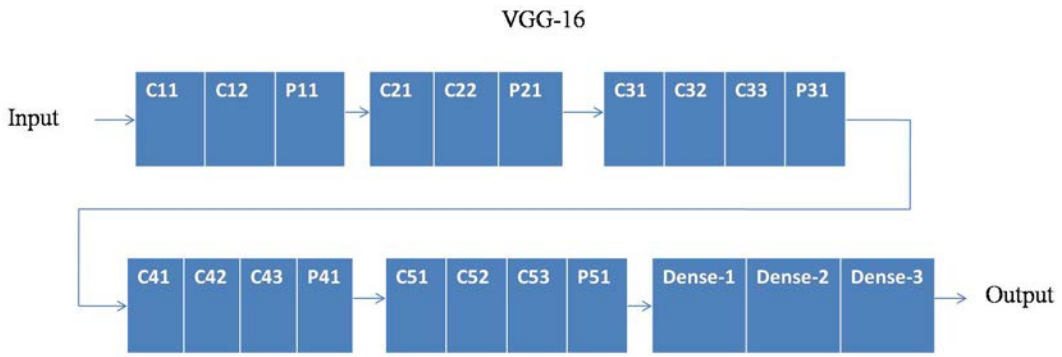

(a)

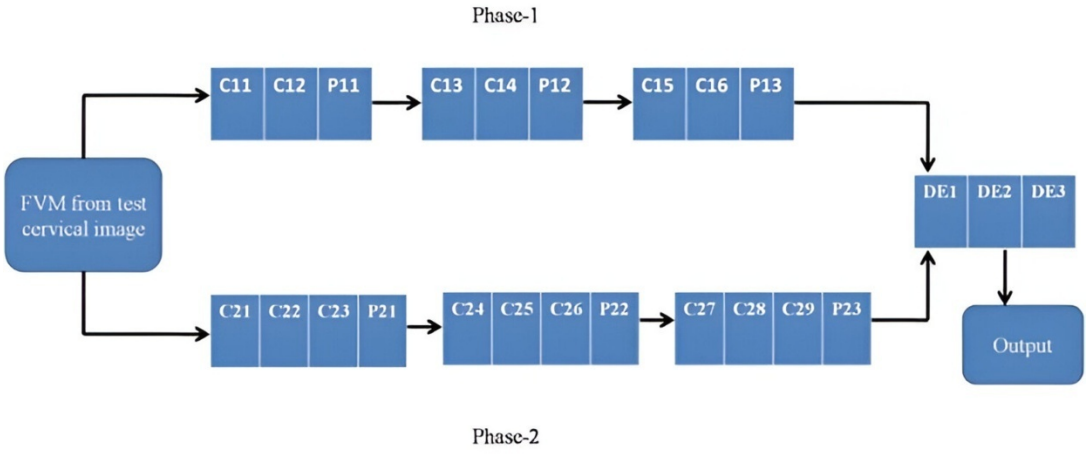

(b)

Fig. 8. (a) Existing VGG-16 model (b) Proposed CFICNN model

Table 3. Layers design specifications of the proposed CFICNN deep learning model

Layers name	Specifications
C11	32 filters, 3×3
C12	32 filters, 3×3
P11	2×2, Max pool
C13	64 filters, 5×5
C14	64 filters, 5×5
P12	2×2, Max pool
C15	128 filters, 7×7
C16	128 filters, 7×7
P13	2×2, Max pool
C21	256 filters, 3×3
C22	256 filters, 3×3
C23	256 filters, 3×3
P21	2×2, Max pool
C24	512 filters, 5×5
C25	512 filters, 5×5
C26	512 filters, 5×5
P22	2×2, Max pool
C27	1024 filters, 7×7
C28	1024 filters, 7×7
C29	1024 filters, 7×7
P23	2×2, Max pool
DE1	4096 neurons
DE2	512 neurons
DE3	2 neurons

The training parameters are the hyper parameters which control the process flow of the proposed CFICNN classifier, which are given in **Table 4**.

Table 4. Training parameters of the proposed CFICNN classifier

Training parameters	Values
Activation function	Sigmoid
Learning algorithm	Adam
Learning rate	0.005
Normalization type	Min-Max Normalization
Epochs	500
Batch size	40
decay	0.01
Loss function	Cross entropy
Drop out rate	0.5
Regularization parameter	0.0001

This research presents a suggested CFICNN deep learning method that classifies the test cervical image output as either abnormal or normal. Next, the aberrant cervical picture is subjected to the morphological segmentation method in order to identify the cancer pixels. The morphological opening and closing functions are applied to the aberrant cervical picture in this algorithm. By subtracting the concluding image from the starting image, one can find the cancer pixels. **Fig. 9** shows the cancer pixels located image.

Fig. 9. Cancer pixels located image

Fig. 10(a) shows Cervigrams being tested, **Fig. 10(b)** shows the proposed segmentation results and **Fig. 10(c)** shows the Manual segmentation output.

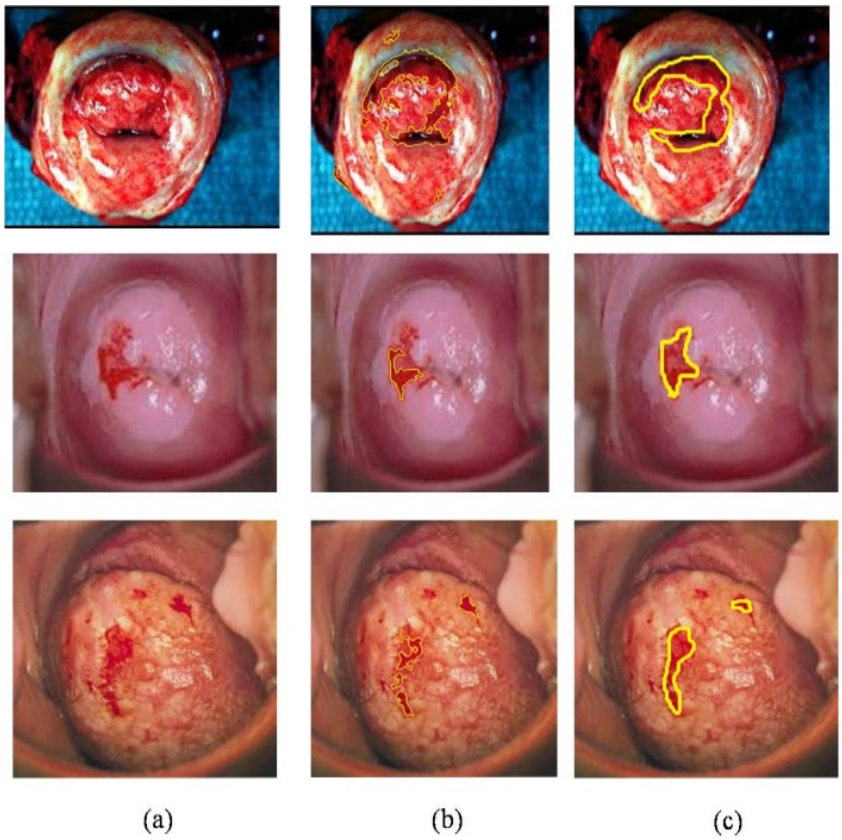

Fig. 10. (a) Cervigrams being tested (b) Proposed segmentation results (c) Manual segmentation output

3. Results and Discussions

This paper uses the cervical images from Guanacaste Dataset (GD) and Kaggle Dataset (KD) for evaluating the performance of the proposed CFICNN based cervical cancer detection system. The entire dataset specifications along with the number of cervical images used in this paper are given in previous section 2.1.

Table 5 shows the illustrations of cervical image dataset on both cervical GD and cervical KD which are used in this paper.

Table 5. Illustrations of cervical image datasets GD and KD with respect to healthy and cancer case

Datasets	Testing cervical images	
	Number of healthy case cervical images	Number of cancer case cervical images
Cervical GD	600	600
Cervical KD	410	102

Cervical Detection Rate (CDR), which is divided into two categories: Healthy Cervical Detection Rate (HCDR) and Cancer Cervical Detection Rate (CCDR), is used to assess the effectiveness of this suggested cervical cancer screening technique. The ratio of correctly identified healthy cervical images to the total number of healthy cervical images is known as

the HCDR. The ratio of accurately identified cancerous cervical images to the total number of cancerous cervical images is known as the CCDR. The values of the HCDR and CCDR are both expressed as percentages and range from 0 to 100. If the suggested cervical cancer detection system achieves higher HCDR and CCDR, its performance efficiency would be good. The following equations show both HCDR and CCDR.

$$HCDR\ (\%) = \frac{\text{Number of healthy cervical images detected correctly}}{\text{Total number of healthy cervical images}} \tag{11}$$

$$CCDR\ (\%) = \frac{\text{Number of cancer cervical images detected correctly}}{\text{Total number of cancer cervical images}} \tag{12}$$

Table 6 shows the computations of HCDR and CCDR for both Cervical GD and KD. In this paper, the proposed CGFCNN method detected 597 healthy cervical images over 600 healthy cervical images and obtains 99.55 HCDR on Cervical GD and also detects 598 cancer cervical images correctly over 600 cancer cervical images which obtain 99.6% CCDR on cervical GD. In this paper, the proposed CGFCNN method detected 407 healthy cervical images over 410 healthy cervical images and obtains 99.2 HCDR on Cervical KD and also detects 100 cancer cervical images correctly over 102 cancer cervical images which obtain 98.0% CCDR on cervical KD.

Table 6. Computations of HCDR and CCDR for both Cervical GD and KD which has been used to analyze the performance efficiency of the proposed CGFCNN system

Datasets	Experimental results					
	Number of healthy case cervical images	**Detected healthy cervical images correctly**	**HCDR (%)**	**Number of cancer case cervical images**	**Detected cancer cervical images correctly**	**CCDR (%)**
Cervical GD	600	597	99.5	600	598	99.6
Cervical KD	410	407	99.2	102	100	98.0

From **Table 6**, the average CDR for the cervical images in GD dataset is about 99.55% and the average CDR for the cervical images in KD dataset is about 98.6%.

The classification algorithm plays an vital role in producing higher CDR values for the cervical images in various datasets. Hence, the impact of these various classification algorithms with respect to machine learning approaches are used in this paper instead of the proposed CGFCNN classification algorithm for the classification process and the experimental results of these existing machine learning approaches are compared more significantly with the proposed CGFCNN in this paper.

Table 7 shows the impact of machine learning models on CDR in both GD and KD dataset cervical images. In this **Table 7**, the proposed CFICNN classifier is performance comparing with other machine learning approaches Support Vector Machine (SVM) classifier, Feed Forward Back Propagation Neural Networks (FFBPNN) classifier, Adaboost classifier and Adaptive Neuro Fuzzy Inference System (ANFIS) classifier with respect to CDR on both GD and KD. In GD cervical image dataset, the existing SVM classifier obtains 94.2% CDR, FFBPNN classifier obtains 93.8% CDR, Adaboost classifier obtains 92.6% CDR and the ANFIS classifier obtains 96.7% CDR. In KD cervical image dataset, the existing SVM

classifier obtains 95.1% CDR, FFBPNN classifier obtains 94.3% CDR, Adaboost classifier obtains 92.9% CDR and the ANFIS classifier obtains 95.9% CDR.

Table 7. Impact and comparative illustrations of various traditional machine learning models on CDR in both GD and KD dataset cervical images

Classification approaches	Average CDR in %	
	GD	KD
Proposed CFICNN classifier	99.55	98.6
SVM classifier	94.2	95.1
FFBPNN classifier	93.8	94.3
Adaboost classifier	92.6	92.9
ANFIS classifier	96.7	95.9

Table 8 shows the impact of existing deep learning models on CDR in both GD and KD dataset cervical images. In this **Table 8**, the proposed CFICNN classifier is performance comparing with other existing deep learning approaches LeNet, AlexNet, Visual Geometry Group (VGG) and Inception network with respect to CDR on both GD and KD. In GD cervical image dataset, the existing LeNet obtains 95.3% CDR, the AlexNet obtains 96.2% CDR, the VGG classifier obtains 96.8% CDR and the inception network obtains 97.3% CDR. In KD cervical image dataset, the existing LeNet obtains 95.1% CDR, the AlexNet obtains 96.1% CDR, the VGG classifier obtains 96.9% CDR and the inception network obtains 97.7% CDR.

Table 8. Impact and comparative illustrations of various traditional Deep learning models on CDR in both GD and KD dataset cervical images

Classification approaches	Average CDR in %	
	GD	KD
Proposed CFICNN classifier	99.55	98.6
LeNet	95.3	95.1
AlexNet	96.2	96.1
VGG	96.8	96.9
Inception Network	97.3	97.7

The following factors are also employed in this paper to examine the performance effectiveness of the suggested cervical cancer detection system, in addition to the CDR parameter.

$$Cervical\ Sensitivity\ Rate\ (CSER) = \frac{TP}{TP+FN} \tag{13}$$

$$Cervical\ Specificity\ Rate\ (CSPR) = \frac{TN}{TN+FP} \tag{14}$$

$$Segmentation\ Accuracy\ Rate\ (SAR) = \frac{TP+TN}{TP+TN+FP+FN} \tag{15}$$

$$Precision\ (P) = \frac{TP}{TP+FP} \tag{16}$$

$$Jaccard\ Index\ (JC) = \frac{TP}{TP+FP+FN} \tag{17}$$

$$Positive\ Predictive\ Rate\ (PPR) = \frac{TP}{TP+FP} \tag{18}$$

$$Negative\ Predictive\ Rate\ (NPR) = \frac{TN}{TN+FN} \quad (19)$$

$$Likelihood\ Ratio\ Positive\ (\text{LRP}) = \frac{CSER}{1-CSPR} \quad (20)$$

$$Likelihood\ Ratio\ Negative\ (\text{LRN}) = \frac{1-CSER}{CSPR} \quad (21)$$

The positively detected cancer and healthy pixels in cervical images are represented as TP and TN and the negatively detected cancer and healthy pixels in cervical images are represented as FP and FN. All these performance index rates are computed by comparing the segmentation experimental results of the proposed cervical cancer detection system with the GS cervical cancer images which are available in both GD and KD datasets. The value of these performance index rates are varied from 0 and 100 and measured in percentage. The higher values of these performance index rates shows that the performance efficiency of the proposed CGFCNN based cervical detection system are high and it is most suitable for the clinical applications in medical field.

Table 9 shows the computation of performance index rates of the cervical images in GD. In this **Table 9**, the cancer cervical images are represented as GD1 to GD10 and they are compared with GS cervical images to compute the performance index rates.

Table 9. Computation of performance index rates of the cervical images in GD through various performance metrics

Cervical Image Sequences	Performance index rate evaluations in %								
	CSER	**CSPR**	**SAR**	**P**	**JC**	**PPR**	**NPR**	**LRP**	**LRN**
GD1	98.6	98.5	98.4	98.8	97.3	98.7	97.3	99.2	97.5
GD2	98.4	98.2	99.3	98.6	98.9	98.3	96.2	99.1	97.3
GD3	98.9	98.1	99.1	99.3	99.1	98.7	95.9	98.8	98.7
GD4	98.5	98.7	99.7	99.2	99.3	98.3	95.3	98.9	98.3
GD5	98.8	99.0	99.6	99.6	99.2	98.1	96.1	99.3	98.6
GD6	99.3	99.2	99.5	99.4	98.9	99.3	96.8	99.1	99.7
GD7	99.1	98.6	99.3	99.1	98.7	99.1	96.3	98.8	99.3
GD8	98.9	98.3	99.8	99.2	99.3	98.2	96.2	98.3	99.1
GD9	98.3	98.7	99.4	99.7	99.8	98.7	96.1	98.1	98.9
GD10	98.2	98.9	99.5	99.4	99.3	98.9	95.6	99.1	98.8
Average	98.7	98.62	99.36	99.23	98.98	98.63	96.18	98.87	98.62

Table 10 shows the computation of performance index rates on KD. In this **Table 10**, the cancer cervical images are represented as KD1 to KD10 and they are compared with GS cervical images to compute the performance index rates.

Table 10. Computation of performance index rates of the cervical images in KD through various performance metrics

Cervical Image Sequences	Performance index rate evaluations in %								
	CSER	CSPR	SAR	P	JC	PPR	NPR	LRP	LRN
KD1	98.3	99.3	98.7	98.6	98.3	98.8	98.4	98.4	98.4
KD2	98.1	99.1	98.3	98.9	98.1	98.4	99.1	98.3	99.1
KD3	99.4	98.9	98.9	99.3	99.3	98.1	99.3	99.1	99.3
KD4	99.7	98.4	99.3	99.1	99.1	98.9	98.7	99.3	98.9
KD5	99.2	98.8	99.1	98.7	99.4	99.3	98.9	98.6	98.5
KD6	99.4	98.2	98.7	98.5	99.7	99.1	98.3	99.5	99.3
KD7	99.7	98.6	98.5	98.9	98.4	98.6	98.1	98.3	99.1
KD8	98.0	99.3	98.9	99.3	98.9	98.3	98.8	98.7	98.6
KD9	98.3	99.1	99.3	99.1	99.3	98.4	98.4	98.5	98.7
KD10	99.1	99.6	99.1	99.5	99.1	98.3	98.8	98.7	98.8
Average	98.92	98.93	98.88	98.99	98.96	98.62	98.68	98.74	98.87

Table 11 shows the comparative analysis of proposed CFICNN classifier with other state of the art methods on GD. The proposed CFICNN based cervical cancer detection system obtains 98.7% CSER, 98.62% CSPR, 99.36% SAR, 99.23% P , 98.98% JC, 98.63% PPR, 96.18% NPR, 98.87% LRP and 98.62% LRN on GD dataset cervical images. In this paper, the experimental results of the proposed CFICNN classifier based cervical cancer detection system is significantly compared with other existing methods Nitin Kumar Chauhan et al. (2023), Umesh Kumar Lilhore et al. (2022), Xin Hou et al. (2022), Alquran et al. (2022), Park et al. (2021) and Ding et al. (2021).

Table 11. Comparative analysis of proposed CFICNN classifier with other state of the art methods on GD to highlight the performance efficiency of the proposed CGFCNN classifier

Methods	Experimental results in %								
	CSER	CSPR	SAR	P	JC	PPR	NPR	LRP	LRN
Proposed CGFCNN classifier	98.7	98.62	99.36	99.23	98.98	98.63	96.18	98.87	98.62
Nitin Kumar Chauhan et al. (2023)	96.8	96.4	96.3	96.7	96.3	96.2	95.9	96.1	95.3
Umesh Kumar Lilhore et al. (2022)	95.2	95.9	95.8	95.9	96.1	95.3	96.1	96.3	95.9
Xin Hou et al. (2022)	94.9	95.6	95.9	94.2	95.3	96.1	94.2	95.2	95.8
Alquran et al. (2022)	95.3	96.1	96.6	96.7	95.9	95.3	96.1	95.9	95.4
Park et al. (2021)	95.1	95.6	95.3	96.1	95.9	95.8	95.3	96.1	95.8
Ding et al. (2021)	94.2	94.8	94.1	94.9	95.1	95.3	95.8	95.8	96.1

Table 12 shows the comparative analysis of proposed CFICNN classifier with other state of the art methods on KD. The proposed CFICNN based cervical cancer detection system obtains 98.92% CSER, 98.93% CSPR and 98.88% SAR, 98.99% P and 98.96% JC, 98.62% PPR, 98.68% NPR, 98.74% LRP and 98.87% LRN on GD dataset cervical images.

Table 12. Comparative analysis of proposed CFICNN classifier with other state of the art methods on KD to highlight the performance efficiency of the proposed CGFCNN classifier

Methods	Experimental results in %								
	CSER	**CSPR**	**SAR**	**P**	**JC**	**PPR**	**NPR**	**LRP**	**LRN**
Proposed CGFCNN classifier	98.92	98.93	98.88	98.99	98.96	98.62	98.68	98.74	98.87
Nitin Kumar Chauhan et al. (2023)	97.9	97.2	96.9	96.1	96.3	95.4	96.3	96.1	95.91
Umesh Kumar Lilhore et al. (2022)	96.3	96.3	95.3	95.8	95.9	96.9	95.3	94.9	95.8
Xin Hou et al. (2022)	96.1	96.9	95.1	96.1	96.7	95.4	95.9	95.3	95.1
Alquran et al. (2022)	95.8	96.5	94.9	95.3	94.9	94.9	94.2	95.8	95.3
Park et al. (2021)	95.1	95.7	95.3	94.3	94.8	94.2	94.8	94.3	94.8
Ding et al. (2021)	94.3	94.1	94.9	94.5	94.9	94.2	94.7	94.1	94.5

3.1 Clinical diagnosis

The proposed fusion based CGFCNN classifier for the cervical cancer detection process have been applied and tested on the two independent cervical imaging datasets and the performance of the system has been analyzed with respect to various parameters in this paper. Though these methods provided optimum experimental results on both open access datasets, the performance has to analyze by the real time clinical imaging datasets. Hence, the proposed methods stated in this paper have been applied on the set of cervical images which have been obtained from the MGM Healthcare, Chennai, India. The image size of this clinical cervical image is about 512 ×512 as image width and height pixel resolution respectively. Totally, 126 cancer cervical images and 267 non-cancer cervical images from this clinical dataset have been used in this paper in order to evaluate the performance of the proposed system on real time imaging environment. This study presents a suggested CGFCNN classifier based cervical cancer detection algorithm that accurately identified 265 cancer cervical images out of 267 cancer cervical images, yielding 99.2% of HCDR. This study presents a suggested CGFCNN classifier based cervical cancer detection algorithm that successfully recognized 124 cancer cervical images out of 126 cancer cervical images, obtaining 98.4% of CCDR. The experimental outcomes of the suggested cervical cancer detection system on the clinical imaging dataset and the suggested cervical cancer detection method on the public cervical imaging datasets are substantially identical.

3.2 Validations

Further, the proposed system experimental results have been validated through the K-fold validation algorithm (Verma et al. 2024).

The K-fold statistical analysis method has been used in this proposed cervical cancer detection. The 5-fold algorithm has been used in this paper. In each fold of this algorithm, five modules are aligned where each module contains 120 numbers of cervical images. During fold-1, module 1 images are tested by the proposed algorithm, where other remaining modules (images) are trained by the proposed classifier. During fold-2, module 2 images are tested by the proposed algorithm, where other remaining modules (images) are trained by the proposed classifier. During fold-3, module 3 images are tested by the proposed algorithm, where other remaining modules (images) are trained by the proposed classifier. During fold-4, module 4 images are tested by the proposed algorithm, where other remaining modules (images) are trained by the proposed classifier. During fold-5, module 5 images are tested by the proposed algorithm, where other remaining modules (images) are trained by the proposed classifier. The average of the CDR has been computed all the folds which is equal to the obtained CDR.. By k-fold algorithm, the CDR parameter of the experimental results of the proposed system is verified.

4. Conclusions

This paper proposes image fusion based cervical cancer detection and segmentation method using cervical images. The proposed method implements the efficient CFICNN deep learning architecture on the computed feature set from the cervical features. This proposed CFICNN classifier produces the classification output and then the segmentation algorithm is applied on the abnormal image to locate the cancer pixels. In this paper, the proposed CGFCNN method detected 597 healthy cervical images over 600 healthy cervical images and obtains 99.55 HCDR on Cervical GD and also detects 598 cancer cervical images correctly over 600 cancer cervical images which obtain 99.6% CCDR on cervical GD. In this paper, the proposed CGFCNN method detected 407 healthy cervical images over 410 healthy cervical images and obtains 99.2 HCDR on Cervical KD and also detects 100 cancer cervical images correctly over 102 cancer cervical images which obtain 98.0% CCDR on cervical KD. The proposed CFICNN based cervical cancer detection system obtains 98.7% CSER, 98.62% CSPR, 99.36% SAR, 99.23% P and 98.98% JC on GD dataset cervical images. The proposed CFICNN based cervical cancer detection system obtains 98.92% CSER, 98.93% CSPR and 98.88% SAR, 98.99% P and 98.96% JC on GD dataset cervical images. The proposed CFICNN classifier is performance comparing with other existing deep learning approaches LeNet, AlexNet, Visual Geometry Group (VGG) and Inception network with respect to CDR on both GD and KD. In this work, the detection and classification of cervical cancer using cervigram images are only performed. Though this method obtained superior performance in terms of various indexing parameters, the Pap smear cell analysis is also important for the same patient to validate the cancer segmentation accuracy. In future, the cervical cancer can be detected by considering both cervigram images and Pap smear cell imaging test using advanced deep learning models. Moreover, the severity estimation and determination is so important for analyzing the performance efficiency of the systematic model. In future direction, the segmented cancer pixels by the proposed CFICNN classifier will be severity diagnosed with respect to the clinical results.

References

[1] M. Kaushik, R. C. Joshi, A. S. Kushwah et al., "Cytokine gene variants and socio-demographic characteristics as predictors of cervical cancer: A machine learning approach," *Computers in Biology and Medicine*, vol.134, 2021. Article(CrossRefLink)

[2] Z. Zhou, G. M. Maquilan, K. Thomas et al., "Quantitative PET Imaging and Clinical Parameters as Predictive Factors for Patients With Cervical Carcinoma: Implications of a Prediction Model Generated Using Multi-Objective Support Vector Machine Learning," *Technology in Cancer Research & Treatment*, vol.19, 2020. Article(CrossRefLink)

[3] S. K. Singh and A. Goyal, "Performance Analysis of Machine Learning Algorithms for Cervical Cancer Detection," *International Journal of Healthcare Information Systems and Informatics*, vol.15, no.2, pp.1-21, 2020. Article(CrossRefLink)

[4] R. Weegar and K. Sundström, "Using machine learning for predicting cervical cancer from Swedish electronic health records by mining hierarchical representations," *PLoS One*, vol.15, no.8, 2020. Article(CrossRefLink)

[5] S. Jahan, M. D. S. Islam, L. Islam et al., "Automated invasive cervical cancer disease detection at early stage through suitable machine learning model," *SN Applied Sciences*, vol.3, no.10, pp.1-17, 2021. Article(CrossRefLink)

[6] A. Jajodia, A. Gupta, H. Prosch et al., "Combination of Radiomics and Machine Learning with Diffusion-Weighted MR Imaging for Clinical Outcome Prognostication in Cervical Cancer," *Tomography*, vol.7, no.3, pp.344-357, 2021. Article(CrossRefLink)

[7] N. K. Chauhan, K. Singh, A. Kumar, S. B. Kolambakar, "HDFCN: A Robust Hybrid Deep Network Based on Feature Concatenation for Cervical Cancer Diagnosis on WSI Pap Smear Slides," *BioMed Research International*, vol.2023, pp.1-17, 2023. Article(CrossRefLink)

[8] U. K. Lilhore, M. Poongodi, A. Kaur, S. Simaiya, A. D. Algarni, H. Elmannai, V. Vijayakumar, G. B. Tunze, M. Hamdi, "Hybrid Model for Detection of Cervical Cancer Using Causal Analysis and Machine Learning Techniques," *Computational and Mathematical Methods in Medicine*, vol.2022, pp.1-17, 2022. Article(CrossRefLink)

[9] X. Hou, G. Shen, L. Zhou, Y. Li, T. Wang, X. Ma, "Artificial Intelligence in Cervical Cancer Screening and Diagnosis," *Front. Oncol*., vol.12, Mar. 2022. Article(CrossRefLink)

[10] H. Alquran, M. Alsalatie, W. A. Mustafa, R. A. Abdi, A. R. Ismail, "Cervical Net: A Novel Cervical Cancer Classification Using Feature Fusion," *Bioengineering*, vol.9, no.10, 2022. Article(CrossRefLink)

[11] Y. R. Park, Y. J. Kim, W. Ju, K. Nam, S. Kim, and K. G. Kim, "Comparison of machine and deep learning for the classification of cervical cancer based on cervicography images," *Scientific Reports*, vol.11, no.1, 2021. Article(CrossRefLink)

[12] D. Ding, T. Lang, D. Zou et al., "Machine learning-based prediction of survival prognosis in cervical cancer," *BMC Bioinformatics*, vol.22, no.1, 2021. Article(CrossRefLink)

[13] P. Charoenkwan, W. Shoombuatong, C. Nantasupha, T. Muangmool, P. Suprasert, and K. Charoenkwan, "iPMI: Machine Learning-Aided Identification of Parametrial Invasion in Women with Early-Stage Cervical Cancer," *Diagnostics*, vol.11, no.8, 2021. Article(CrossRefLink)

[14] M. Patil, S.V. Deshmukh, "The Machine Learning Algorithm for Prediction of Risk Factors of Cervical Cancer," *International Journal for Research in Applied Science & Engineering Technology (IJRASET)*, vol.9, no.VI, pp.4177-4180, 2021. Article(CrossRefLink)

[15] M. Glučina, A. Lorencin, N. Anđelić, I. Lorencin, "Cervical Cancer Diagnostics Using Machine Learning Algorithms and Class Balancing Techniques," *Applied Sciences*, vol.13, no.2, 2023. Article(CrossRefLink)

[16] O. E. Aina, S. A. Adeshina, and A.M. Aibinu, "Deep Learning for Image-based Cervical Cancer Detection and Diagnosis - A Survey," in *Proc. of 2019 15th International Conference on Electronics, Computer and Computation (ICECCO)*, pp.1-7, Abuja, Nigeria, 2019. Article(CrossRefLink)

[17] M. Wu, C. Yan, H. Liu, Q. Liu, and Y. Yin, "Automatic classification of cervical cancer from cytological images by using convolutional neural network," *Bioscience Reports*, vol.38, no.6, 2018. Article(CrossRefLink)
[18] S. K. Mathivanan, D. Francis, S. Srinivasan et al., "Enhancing cervical cancer detection and robust classification through a fusion of deep learning models," Scientific Reports, vol.14, 2024. Article(CrossRefLink)
[19] N. Dong, L. Zhao, C.H. Wu, and J.F. Chang, "Inception v3 based cervical cell classification combined with artificially extracted features," *Applied Soft Computing*, vol.93, 2020. Article(CrossRefLink)
[20] W. Hua, T. Xiao, and X. Jiang et al., "Lymph-vascular space invasion prediction in cervical cancer: Exploring radiomics and deep learning multilevel features of tumor and peritumor tissue on multiparametric MRI," *Biomedical Signal Processing and Control*, vol.58, 2020. Article(CrossRefLink)
[21] V. K. Verma, K. Saxena, U. Banodha, "Analysis Effect of K Values Used in K Fold Cross Validation for Enhancing Performance of Machine Learning Model with Decision Tree," in *Proc. of Advanced Computing, 13th International Conference, IACC 2023*, Communications in Computer and Information Science, vol.2053, pp.374-396, Springer, Cham, 2024. Article(CrossRefLink)

I. Dhurgabai completed her bachelor degree in Electronics and Communication Engineering at Udaya School of Engineering, Kanyakumari in 2009 and Master degree in Communication Systems at Anna University, Madurai Regional Campus. She is currently working as Assistant professor at Theni Kammavar Sangam College of Technology. Her areas of research include Image Processing and Medical imaging.
E-mail: idhurgabaiphd@gmail.com

Selvapandian Arumugam completed his bachelor degree in Electronics and Communication Engineering at RVSCET, Dindigul in 2009 and Master degree in VLSI Design at PSNACET, Dindigul. He completed his doctorate in the year of 2020 under Anna University and is currently working in ECE department at Gnanamani college of Technology. His areas of research include Image Processing and Segmentation, Medical imaging.
E-mail: selvapandian@gct.org.in